Journal of The Electrochemical Society, **155** (5) D369-D376 (2008) D369
0013-4651/2008/155(5)/D369/8/$23.00 © The Electrochemical Society

Investigation of Electroless Co(W,P) Thin Film as the Diffusion Barrier of Underbump Metallurgy

W. C. Wu, Tsung-Eong Hsieh,[z] and Hung-Chun Pan

Department of Materials Science and Engineering, National Chiao Tung University, Hsinchu, 30010 Taiwan

The plating characteristics of an electroless cobalt–tungsten–phosphorus [Co(W,P)] layer and its capability to serve as a diffusion barrier of underbump metallurgy (UBM) for flip-chip Cu–IC are investigated. Increasing the pH of the plating solution in a range of 7.6–9.0 decreased the rate of deposition, increased the phosphorus content, altered the structure from polycrystalline to amorphous, and decreased the surface roughness of Co(W,P) films. The barrier capability of Co(W,P) to eutectic PbSn solder was evaluated by means of liquid- and solid-state aging tests. In specimens subjected to tests of these two types, a P-rich layer presented in between solder and unreacted Co(W,P), demonstrating the sacrificial barrier behavior of Co(W,P). Transmission electron microscopy (TEM) analysis of specimens subjected to liquid-state aging indicated the supersaturated P atoms, and the Co_2P consequently formed, might aggregate at grain boundaries of the P-rich layer, thus enabling the stuffed-type barrier capability of the Co(W,P) layer. TEM, scanning electron microscopy, and energy-dispersive spectrometer characterizations of specimens subjected to solid-state aging revealed that the reaction of solder and Co(W,P) implies a formation of $CoSn_2$ and $CoSn_3$ intermetallic compounds (IMCs) and a mixture of various IMCs in P-rich layer. Our experimental results demonstrated a satisfactory barrier property of electroless Co(W,P), heralding promising applications in UBM structures for flip-chip Cu–IC.
© 2008 The Electrochemical Society. [DOI: 10.1149/1.2885083] All rights reserved.

Manuscript submitted March 9, 2007; revised manuscript received January 25, 2008. Available electronically March 12, 2008.

The underbump metallurgy (UBM) structure is divisible into an adhesion layer, a diffusion barrier layer, and a wetting layer or antioxidation layer. According to Nicolet, the diffusion barrier is classifiable as a sacrificial barrier, stuffed barrier, passive-compound barrier, or amorphous barrier.[1] The most common materials used in UBM as a diffusion barrier layer are refractory metals, such as titanium (Ti), tungsten (W), molybdenum (Mo), and their alloys, which have effective adherence and a superior capability as a diffusion barrier. Physical vapor deposition (PVD), such as sputtering, is conventionally adopted to prepare a UBM structure, but in recent submicrometer Cu–IC processes, the thin films prepared with PVD suffer from poor step coverage.[2] Another popular diffusion barrier material is electroless Ni because of its low-stress status relative to Ni produced by sputtering.[3] Moreover, amorphous electroless Ni has no grain boundaries for short-circuit diffusion and exhibits effective barrier properties.[4-7] The electroless process allows a parallel processing of multiple wafers at low temperature and has a large yield. It is a promising technique for the current 60 nm Cu–IC process and electronic packaging applications because minimal cost is perennially a key issue in production.

Electroless Co(P) exhibited a superior barrier capability to counter the interdiffusion between Cu and the interlayer dielectric (ILD) in Cu–IC relative to electroless Ni(P) and, for a thickness only 50 nm, electroless Co(P) remained an effective diffusion barrier layer up to 400°C.[8] Moreover, it possesses a small sheet resistance and an effective step coverage, and has a potential to replace conventional barrier layers for Cu–IC, such as Ta and TaN.[9] Our previous work confirmed that the electroless Co(P) film might also impede interdiffusion between eutectic PbSn solder and Cu elements.[10] Other research[11-13] revealed that the enhanced thermal property and capability as a diffusion barrier of Co(W,P) films are due to the existence of elemental W in those thin films. Electroless Co(W,P) was hence considered a material for a diffusion barrier better than Co(P), but related work on the feasibility of electroless Co(W,P) as a barrier in UBM is unavailable. Our objective was thus to investigate the plating characteristics of a Co(W,P) film and its barrier capability against elemental inter-diffusion to evaluate its applicability to a UBM structure of flip-chip Cu–IC.

[z] E-mail: tehsieh@cc.nctu.edu.tw

Experimental

Sample preparation.— Si wafers cleaned according to the RCA process were adopted as sample substrates. After an oxide layer on the wafer surface was formed through wet oxidation, a Ti/Cu layer simulating the Cu interconnect was deposited by e-beam evaporation. Before electroless deposition, the substrate surface was subjected to roughening/sensitization/activation treatments according to the methods and solutions listed in Table I. After a Pd catalytic layer was formed on the substrates, electroless plating of a Co(W,P) layer was performed using the solutions defined in Table II. A plating solution (1 L) was effective for the deposition of a Co(W,P) layer (thickness of ~ 2 μm, plating for ~ 2.5 h) with the desired composition. In this experiment, our plating conditions are pH 7.6–9.0, temperature = 90 ± 2°C, V/A (the ratio of plating solution volume to the plating surface area in microliters per centimeters squared) ≥ 100; the duration of plating was adjusted with respect to the required layer thickness. During plating, the pH of the solution was monitored with a pH meter and regulated with a KOH solution (3 M). With a surface profiler (KLA-TENCOR P-10), we measured the specimens subjected to varied durations of plating, and the rate of plating was calibrated accordingly. To achieve an electroless Co(W,P) film with a desired microstructure and uniform composition, it is important to modulate the concentration of the plating solution constantly during deposition. After electroless plating, the substrates containing Co(W,P) were washed with deionized water and blown dry with a N_2 jet. The PbSn solder paste of eutectic composition was immediately applied to the substrates, and a brief reflow at 250°C was performed to solidify the solder. For subsequent tests of interdiffusion, the vacuum-sealed PbSn solder/Co(W,P)(3–5 μm)/Cu(1 μm)/Ti(0.2 μm)/SiO_2(0.3 μm)/Si specimens were placed in a furnace at 250°C (liquid-state aging test) or 150°C (solid-state aging test) for various durations of ther-

Table I. Solutions and duration of immersion for roughening, sensitization, and activation

Step	Component	Concentration	Duration of immersion
Roughening	H_2SO_4	5 wt %	30 s
Sensitization	$SnCl_2 \cdot 2H_2O$	10 g/L	5 min
	HCl	40 ml/L	
Activation	$PdCl_2$	0.1 g/L	1 min
	HCl	8 ml/L	

Table II. Composition of electroless plating bath.

Component	Concentration (g/L)
$CoSO_4 \cdot 7H_2O$	23
$NaH_2PO_2 \cdot H_2O$	18
Na_3 citrate	144
H_3BO_3	31
$Na_2WO_4 \cdot 2H_2O$	10
pH	7.6–9.0

mal treatment. Afterward, analyses with regard to the interfacial reactions between the Co alloy layers and solder were conducted.

Microstructure and composition characterizations.— The crystal structures of electroless Co(W,P) films were characterized with a X-ray diffractometer [(XRD), M18 XHF, MacScience] operated at 200 mA and 50 kV. The source of X-ray was Cu K_α radiation (wavelength 0.154 nm), and the rate of scanning for signal acquisition was 4°/min. We used a transmission electron microscope [(TEM), Philips Tecnai F20] and a scanning electron microscope [(SEM); field emission–SEM (FE-SEM), JSM-6500F; or FE-SEM Hitachi S-4700] in conjunction with an energy-dispersive spectrometer [(EDX), Oxford Inca Energy 300] to examine the surface morphology, microstructure, and evolution of intermetallic compounds (IMCs) in each specimen. Cross-sectional TEM (XTEM) specimens were prepared with a focused-ion-beam [(FIB), FEI-201] technique supported by Materials Analysis Technology, Inc., Chupei, Taiwan. An SEM/EDX line scan was adopted to analyze the composition profiles of cross-sectional specimens subjected to varied durations of liquid- or solid-state aging tests. To obtain an average composition for subsequent discussion, we measured at least four locations for each specimen with EDX analysis.

Results and Discussion

Characterization of electroless Co(W,P) films.— Effect of pH on the rate of deposition.— Figure 1 illustrates the thickness of Co(W,P) films as a function of plating duration deposited under conditions pH 8.0, 8.6, and 9.0. The rate of plating of electroless Co(W,P) decreases with increased pH. The electrochemical reactions involved in electroless Co plating are written as[14]

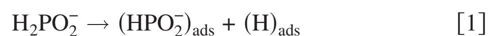

$$H_2PO_2^- \rightarrow (HPO_2^-)_{ads} + (H)_{ads} \quad [1]$$

$$(HPO_2^-)_{ads} + OH^- \rightarrow H_2PO_3 + 2e^- \quad [2]$$

$$Co^{2+} + 2e^- \rightarrow Co \quad [3]$$

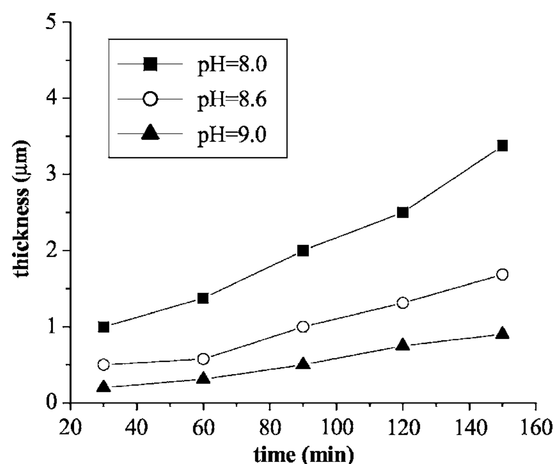

Figure 1. Thickness of electroless Co(W,P) layers deposited at varied pH as a function of duration of plating.

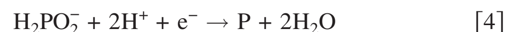

$$H_2PO_2^- + 2H^+ + e^- \rightarrow P + 2H_2O \quad [4]$$

Electrochemical reactions depicted in Eq. 2 and 3 indicate that a large pH promotes the release of electrons and, hence, the deposition of elemental Co, in contrast with the result shown in Fig. 1. Examining the effect of pH on the rate of deposition of electroless Co(W,P), Paunovic et al. found that plots of rate of deposition vs pH of plating solution form concave-downward curves (i.e., the rate of deposition first increases with increasing pH, attains a maximum, and then decreases with further increasing pH).[15] Their work indicated that, in a medium at large pH, hydroxyl ions (OH^-) become a dominant factor in the kinetics of plating by decreasing the charge-transfer coefficient (i.e., the probability of an electron and metal ion combining, thereby triggering the plating), producing a decreased rate of deposition. We speculate that the pH of the present work falls into the range of large pH proposed by Paunovic et al. Although the rate of deposition was low, we observed that Co(W,P) films deposited at large pH exhibited shiny and bright surfaces. A flat surface implies an effective densification of Co(W,P) films, which, in turn, is beneficial for their subsequent barrier performance.

The rate of plating deduced from Fig. 1 also affects the uniformity and quality of the Co(W,P) layer. Figures 2a and b show the morphology of Co(W,P) layers deposited at pH 8.0 and 9.0, respectively. Although the plating solution at pH 8.0 exhibited a rapid rate of plating, it produced a loosely deposited layer with a rough surface profile. According to the electrochemical reactions stated above, a rapid rate of plating implies a fast rate of release of gaseous hydrogen. If adsorbed hydrogen bubbles are not removed appropriately, they become voids trapped in an electroless layer as the plating proceeded, resulting in numerous pinhole defects shown in Fig. 2a that might act as channels of undesired alloy reactions in subsequent aging tests and thus inhibiting a systematic analysis of the barrier

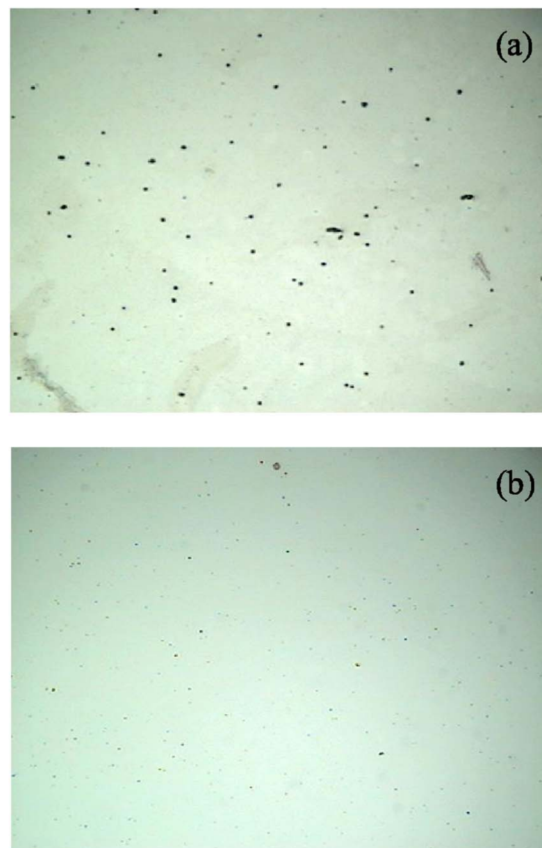

Figure 2. (Color online) Morphology of Co(W,P) layers deposited at pH (a) 8.0 and (b) 9.0 taken by optical microscopy (magnification=100×).

capability of Co(W,P). The Co(W,P) layer deposited at a low plating rate (i.e., pH 9.0) exhibits a smooth surface and satisfactory film quality, as illustrated in Fig. 2b, but the low plating rate adversely affects the preparation of a sufficiently thick Co(W,P) layer. In preparing the Co(W,P) layer for UBM applications, a compromise hence exists between the rate of plating and film uniformity.

Effects of pH on microstructure and composition.— Figure 3 depicts the XRD patterns of Co(W,P) films plated at a pH in a range of 7.6–9.0. The three most intense peaks corresponding to hexagonal ε-phase Co, $(10\bar{1}0)$ at $2\theta = 41.68°$, (0002) at $2\theta = 44.76°$, and $(10\bar{1}1)$ at $2\theta = 47.57°$, indicate that the polycrystalline structure constitutes a Co(W,P) layer deposited at small pH. The gradual diminution of these characteristic features with increasing pH indicates the emergence of nanocrystalline, and eventually amorphous, structure in Co(W,P) films.

Figures 4a and b show XTEM micrographs of Co(W,P) layers deposited at pH 7.6 and 8.6, respectively. As Fig. 4a shows, the Co(W,P) layer deposited at pH 7.6 possesses a columnlike granular structure with lateral size of <100 nm. The spotted ring pattern decorated with random bright spots present in the attached selected-area electron-diffraction (SAED) pattern clearly illustrates that the Co(W,P) layer deposited at pH 7.6 is polycrystalline. For the Co(W,P) layer deposited at pH 8.6, the faint background without distinct contrast in its TEM image and the vague diffraction rings in the attached SAED pattern indicate that such a Co(W,P) layer is essentially amorphous. During the characterization of such a TEM specimen, diffraction rings with uneven brightness in SAED patterns emerged on some occasions, and the corresponding TEM image at large magnification exhibits a lattice fringelike contrast, as shown in Fig. 4c. There seemed to be a few nanocrystalline granules embedded in the amorphous Co(W,P) layer. According to EDX attached to TEM, adopted to undertake a composition analysis, the P and W contents in the Co(W,P) layer deposited at pH 8.6 were in ranges of 9.1–10.2 atom % and 0.4–0.9 atom %, respectively. Previous works[11-13] reported that electroless Co(W,P) films containing 8–10 atom % of P are nanocrystalline, a mixture of nanocrystalline and amorphous structures for a P content within 10–12 atom %, and the films are entirely amorphous for a P content exceeding 12 atom %. According to the above TEM characterizations and the SEM/EDX composition analyses summarized in Fig. 4, the evolution of microstructure with P content in our electroless Co(W,P) layers agrees satisfactorily with that reported previously.[11-13]

Figure 5 presents the composition of Co(W,P) layers deposited at varied pH, analyzed with SEM/EDX. With increasing pH of the plating solution, the P content increases, whereas the W and Co contents decrease in the Co(W,P) layers. The simultaneous decrease of Co and W contents with increasing pH is attributed to the OH^--related kinetics[15] stated in the preceding section and to a codeposition phenomenon.[14] The variation of P content is explained based on the reduction reactions depicted in Eq. 3 and 4, which show Co^{2+} and $H_2PO_2^-$ to compete for electrons during plating. As the Co deposition was retarded by the OH^--related kinetics, more

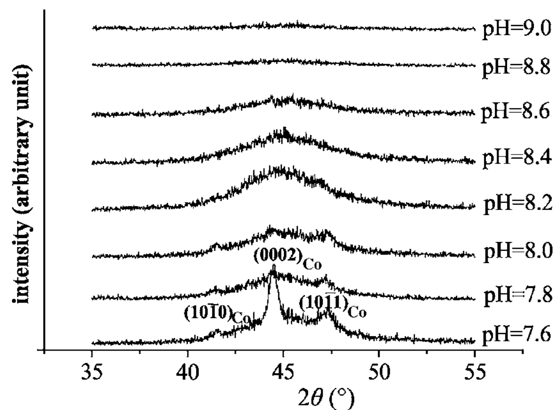

Figure 3. XRD patterns of Co(W,P) films plated at varied pH of plating solution.

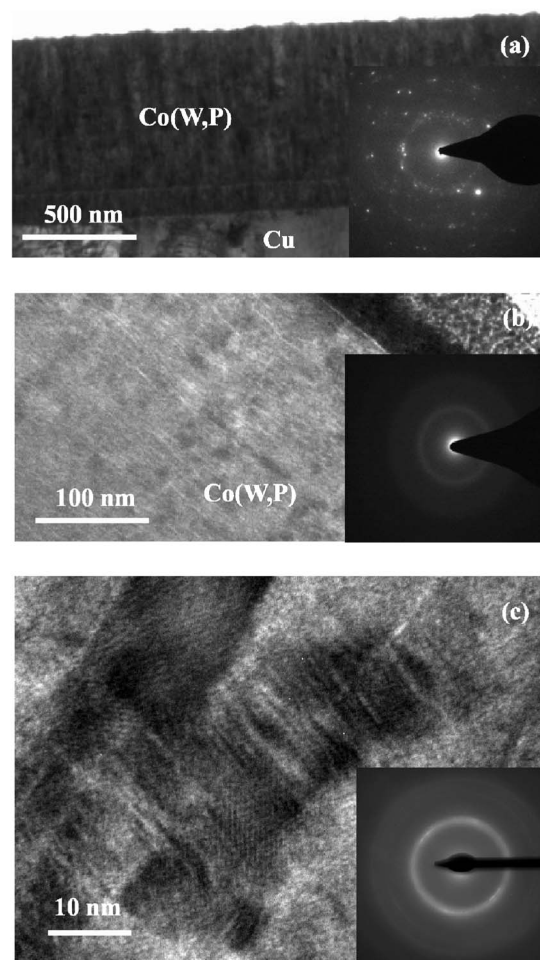

Figure 4. XTEM images of Co(W,P) layers deposited at pH (a) 7.6 and (b) 8.6. The image shown in (c) is an enlargement of the area with dark contrast in (b).

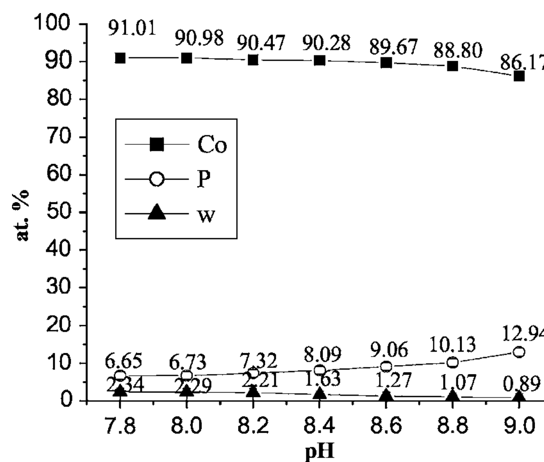

Figure 5. Relation between the composition of a Co(W,P) film and pH of the plating solution.

electrons were available to react with $H_2PO_2^-$, and hence, more elemental P was precipitated. The P content hence increases with decreasing Co content in electroless Co(W,P) films in the chosen pH range of the present work.

Effects of duration of plating and surface morphology.— Figures 6a-c present the surface morphologies of Co(W,P) films deposited at pH 8.6 for various durations of plating. Spherical granules comprise the electroless Co(W,P) films and their grain sizes increase with duration of plating. All electroless Co(W,P) films prepared in the present work exhibited a surface morphology similar to that shown in Fig. 6, and spherical granules do not necessarily imply crystalline Co(W,P) grains. Their microstructure was set by the plating conditions (e.g., the pH of the plating solution). Such a spherical granular surface morphology was attributed to dispersed Pd-island clusters on an activated substrate surface that initialized subsequent Co plating reaction.[16] During plating, the granules grew and coalesced with each other; a grain coarsening was thus observed with an increased duration of plating.

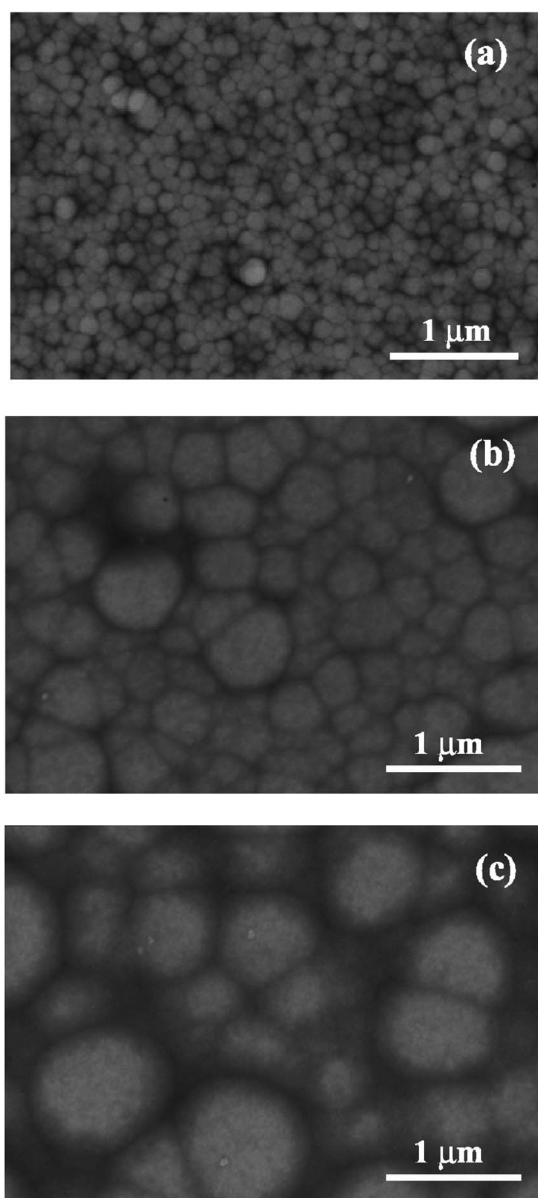

Figure 6. Surface morphologies of Co(W,P) films deposited at pH 8.6 for (a) 10 min, (b) 1, and (c) 3 h.

Interfacial reactions between electroless Co(W,P) and PbSn solder.— Liquid-state aging test.— Figure 7a shows a cross-sectional SEM view of an as-deposited PbSn solder/Co(W,P) sample. A sample subjected to liquid-state aging at 250°C for 40 min is shown in Fig. 7b. The thin lathlike phases embedded in the solder were identified as $CoSn_2$ intermetallic compound (IMC) via EDX analysis, conforming to the prediction of the Co–Sn binary phase diagram.[17,18] The randomly dispersed IMCs result from spallation of IMC growing from the solder/Co(W,P) interface. Although the Co–Sn binary phase diagram predicts also the α-Co_3Sn_2, CoSn and $CoSn_3$ phases,[17,18] throughout the investigation our SEM/EDX characterizations rarely detected those IMC types in samples subjected to liquid-state aging. We speculate that, as Co atoms diffuse to react with Sn in solder, a P-rich layer gradually forms at the

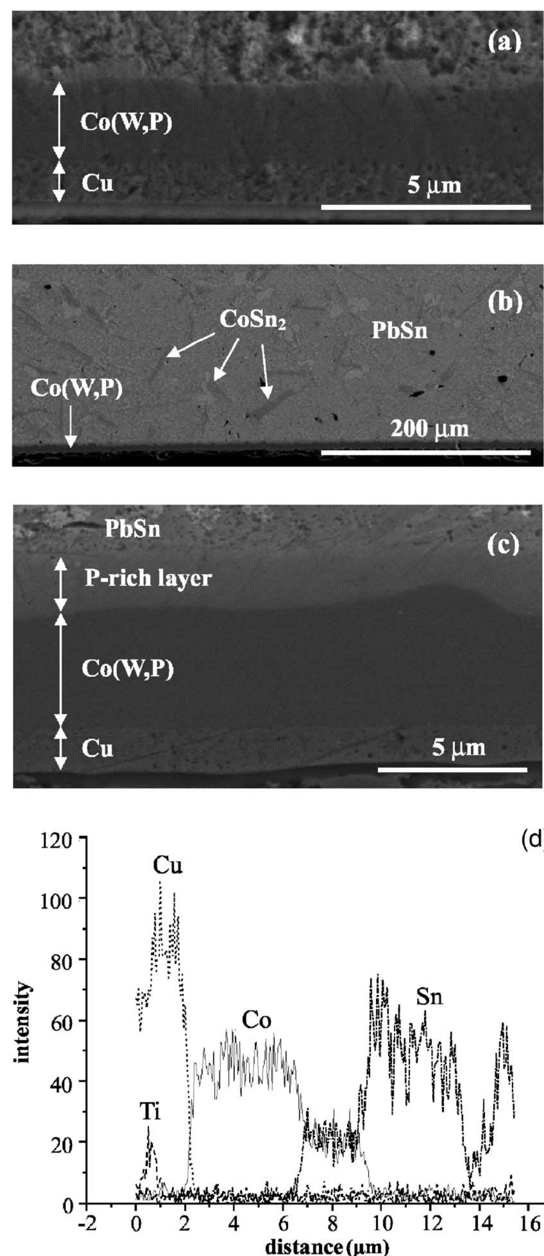

Figure 7. Cross-sectional SEM images of a solder/Co(W,P) interface subjected to liquid-state aging test: (a) the as-deposited sample; (b) the spallation of $CoSn_2$ IMCs in the PbSn solder; (c) enlargement of the solder/Co(W,P) interface; and (d) EDX line scanning of (d). The electroless Co(W,P) was deposited at pH 8.6.

IMC/Co(W,P) interface through the accumulation of elemental P and W (see Fig. 7c and related discussion that follows). When the P-rich layer becomes thick enough to block a further supply of Co, formation of Co-rich IMC phases (i.e., α-Co_3Sn_2 and CoSn) is thus precluded. As to the Sn-rich $CoSn_3$ phase, both SEM and TEM characterizations revealed its existence in samples subjected to solid-state aging (see discussion in next section). According to the phase diagram proposed by Jiang et al.,[18] $CoSn_2$ and $CoSn_3$ are related according to a peritectic reaction expressed as

$$\beta\text{-}Sn_{(l)} + CoSn_{2(s)} \leftrightarrow CoSn_{3(s)} \quad [5]$$

During heating, $CoSn_3$ decomposes into liquid-state β-Sn and $CoSn_2$ as $CoSn_3$ is a less stable phase. Although Co might react with solder to form $CoSn_3$, according to the peritectic reaction, it likely transforms into $CoSn_2$ when spalling into the molten solder during liquid-state aging. The peritectic reaction proceeds in a reverse direction during cooling, during which nuclei of $CoSn_3$ would supposedly grow from the surface of $CoSn_2$, but when the sample is cooled down to room temperature, the solder solidifies and the rate of diffusion becomes so low that the peritectic reaction is essentially terminated. The spalled IMC might have a core-shell structure composed of $CoSn_3$ and $CoSn_2$, but most of it would be identified as $CoSn_2$ because of the relatively small proportion of shell-like $CoSn_3$ on $CoSn_2$.

Figure 7c presents an enlarged SEM image of the solder/Co(W,P) interface, of which a notable feature is the light-gray layer (thickness of ~2 μm) between the solder/IMC and the unreacted Co(W,P) layer. EDX analysis identified this layer as a P-rich (~20 atom %) region mixed with elemental Pb, Sn, Co, P, and W. Previous work reported an accumulation of phosphorus at the PbSn/Ni(P) interface because of the low solubility of P in solder; when the content of P is sufficient, a Ni_3P IMC might form.[19] The analytical results above reveal a similar behavior of electroless Co(W,P) in that its reactions with molten solder also induce an accumulation of elemental P at the IMC/Co(W,P) interface. The excessive P atoms consequently react with Co to form a cobalt phosphide IMC, such as Co_2P, as predicted in the Co–P binary-alloy phase diagram.[17] The microstructure and phase types in the Co(W,P) layer subjected to the liquid-state aging were also characterized with TEM and are presented below.

A line scan of EDX elements was performed for elemental Ti, Cu, Co, and Sn alongside the SEM image shown in Fig. 7c; the result is presented in Fig. 7d. The variation of elemental signals clearly indicates that the electroless Co(W,P) successfully retards the interdiffusion of Sn and Cu.

A sample containing an electroless Co(W,P) layer deposited at pH 8.0 was also prepared for a liquid-state aging test. According to the results presented in a previous section, the Co(W,P) layer deposited at pH 8.0 tends to be polycrystalline, whereas the Co(W,P) layer deposited at pH 8.6 is essentially amorphous. As shown in Fig. 8a and b, the SEM characterization, in conjunction with an EDX element line scan, revealed that the electroless Co(W,P) deposited at pH 8.0 exhibits a barrier behavior similar to that deposited at pH 8.6. Regardless of the microstructure, both electroless Co(W,P) layers successfully inhibit interdiffusion between Sn and Cu. In both cases, a P-rich layer (thickness of ~2 μm) formed due to the interactions of Co(W,P) and molten solder and inhibited further diffusion of solder. The consumption Co(W,P) is evidenced by the significant amount of Sn in P-rich layer as depicted in Fig. 7d and 8b, demonstrating the feature of a sacrificial type barrier for electroless Co(W,P).

The EDX analyses presented above also show that Cu can barely diffuse into electroless Co(W,P). This is attributed to elemental P and W and consequently formed phosphide phase segregated at the boundaries of nanograins in electroless Co(W,P) that effectively retard the diffusion of Cu. The XRD characterization of a Co(W,P) layer subjected to annealing at 250°C for various durations presented in Fig. 9 illustrates that the recrystallization of Co(W,P) becomes obvious after thermal aging for 20 min. Figure 10 shows a XTEM image of a Co(W,P) layer in a sample subjected to a liquid-state aging test for 40 min. A netlike structure constituted by dark, irregularly shaped precipitates with a size of ~20 nm is discernible. The inserted SAED pattern indicates that the Co(W,P) becomes polycrystalline, consistent with the XRD analysis presented in Fig. 9. Furthermore, the indexing of the SAED pattern indicates the for-

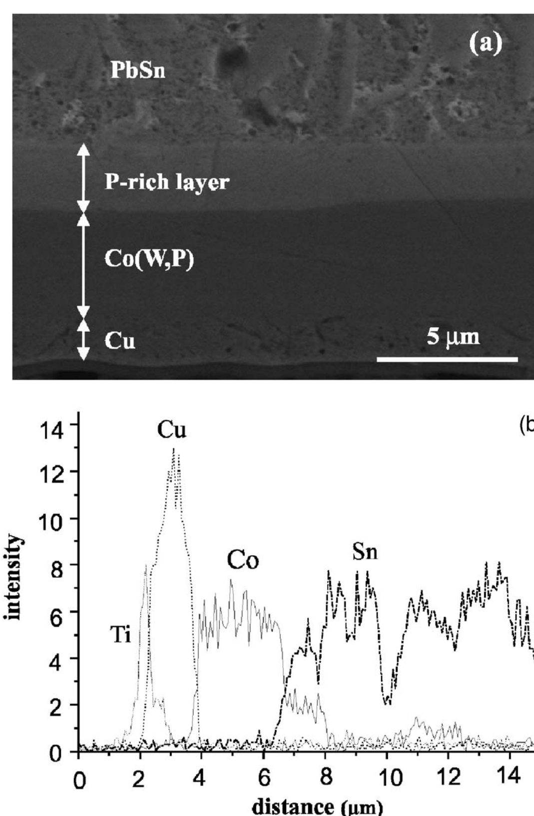

Figure 8. (a) Cross-sectional SEM image of the solder/Co(W,P) interface and (b) the corresponding EDX line scanning. The electroless Co(W,P) was deposited at pH 8.0.

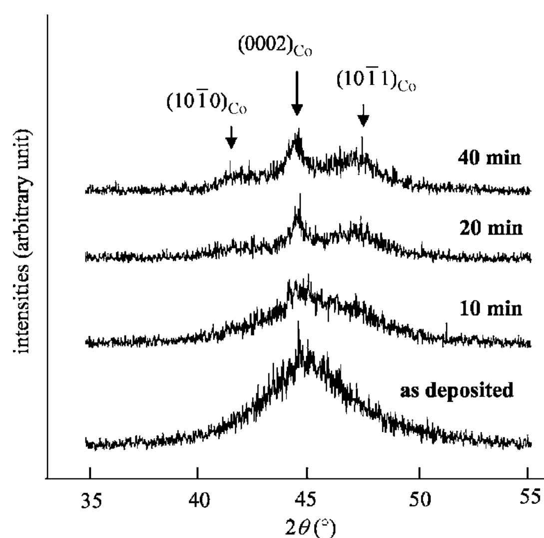

Figure 9. XRD patterns of a Co(W,P) film subjected to annealing at 250°C for various durations. The electroless Co(W,P) was deposited at pH 8.6.

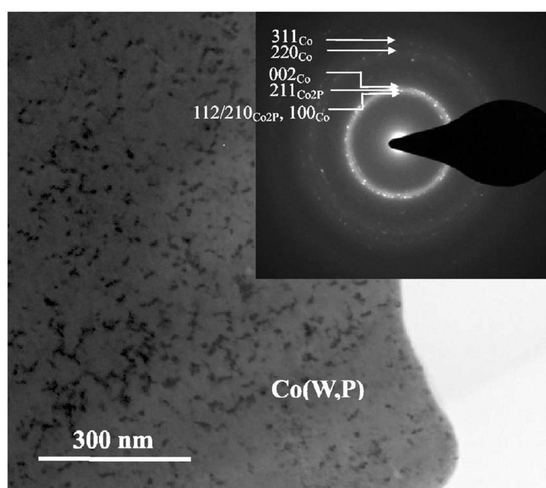

Figure 10. XTEM image of a Co(W,P) layer subject to a liquid-state aging test for 40 min.

mation of a Co_2P phase. We speculate that thermal aging promotes the diffusion of supersaturated P atoms that tend to accumulate at the boundaries, corners, and triple junctions[20] of nanograins. The P atoms might further react with Co to form a phosphide phase during recrystallization of Co(W,P). This process provides the stuffed-type feature of an electroless Co(W,P) layer, which, in turn, suppresses short-circuit diffusion along grain boundaries in polycrystalline Co(W,P). In conjunction with SEM analysis presented above, we conclude that, in practical UBM applications, the electroless Co(W,P) constitutes a barrier of combined type (i.e., a combination of sacrificial and stuffed-type barrier). Further evidence is provided in the next section delineating the solid-state aging test.

To explore the role of W element on barrier property, we also performed a liquid-state aging on PbSn solder/electroless Co(P) samples. SEM/EDX analysis revealed that the electroless Co(P) has a barrier behavior similar to that of electroless Co(W,P) despite that more Co(P) is consumed to form a P-rich layer (thickness of $\sim 3\ \mu m$). The presence of W hence effectively suppresses the alloy reactions of solder and Co; its addition thus benefited the barrier capability of the electroless Co layer.

Solid-state aging test.— Figures 11a and b present cross-sectional SEM micrographs of the solder/Co(W,P) interface subjected to a solid-state aging test at 150°C for 200 and 1000 h, respectively. By EDX analysis we identified the acicular aggregates growing from the solder/Co(W,P) interface into the solder as a mixture of $CoSn_2$ and $CoSn_3$ IMCs. $CoSn_2$ dominates, however, in the bottom part of the IMC [i.e., the region neighboring unreacted Co(W,P)], whereas $CoSn_3$ is commonly detected in the upper portion of the IMC that grow into solder. The light-gray layer underneath the IMC phases is a P-rich layer, a situation similar to the case in the liquid-state aging test, whereas the dark-gray layer beneath the P-rich layer is Co(W,P) that remained intact after annealing at 150°C prolonged up to 1000 h. In both liquid- and solid-state aging tests, we observed the alloy reactions of solder and Co(W,P) to form a P-rich layer of $\sim 2\ \mu m$ thick. An electroless Co(W,P) layer with sufficient thickness (e.g., $\geq 2\ \mu m$) is thus required for it to be adopted as a diffusion barrier layer in an UBM structure.

As illustrated in Fig. 11c, the EDX line scan on a specimen subjected to annealing at 150°C for 1000 h indicates the effectiveness of electroless Co(W,P) serving as a diffusion barrier. In conjunction with the results of a liquid-state aging test presented previously, this result corroborates the superior barrier capability of electroless Co(W,P) films for a UBM applied to flip-chip Cu–IC.

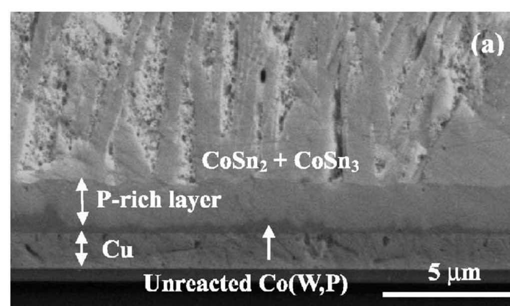

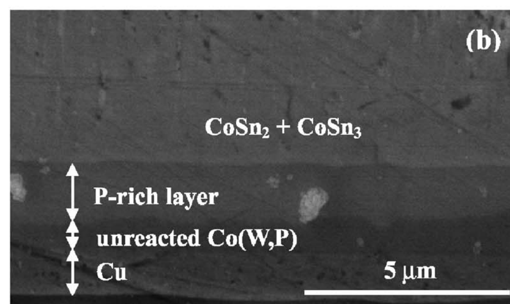

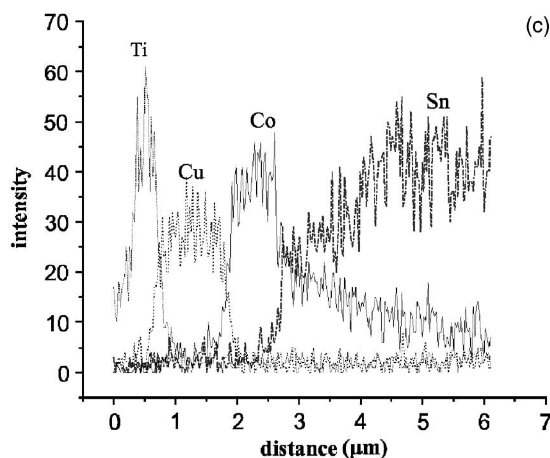

Figure 11. Cross-sectional SEM image of the solder/Co(W,P) interface subjected to solid-state aging test at 150°C for (a) 200 (b) 1000 h, and (c) the corresponding EDX line scanning for (b).

XTEM images of a sample subjected to aging for 1000 h, and an enlarged portion of the Co(W,P) layer are shown in Fig. 12a and b, respectively. Composition analysis utilizing EDX attached to the TEM revealed that the reaction of solder and Co(W,P) implies the formation of $CoSn_2$ and $CoSn_3$ IMCs, confirming the results obtained with SEM/EDX shown in Fig. 11. Notable features in Fig. 12b include the presence of ultrafine precipitates dispersed in the Co(W,P) layer, and that the Co(W,P) neighboring IMCs is polycrystalline, whereas the Co(W,P) adjacent to the Cu underlayer remains mostly amorphous as indicated by attached SAED patterns. As shown in Fig. 12c, the ring indices of the SAED pattern taken from the part of Co(W,P) neighboring the IMCs (i.e, the upper part of Fig. 12b) indicate the plausible existence of a complicated IMC mixture including α-$CoSn_3$, β-$CoSn_3$, $CoSn_2$, Co_2P, etc., in the P-rich regime. We speculate that the elements in solder and Co(W,P) react with each other to form various IMCs with specific crystallinities during solid-state aging. With the progress of the aging test, the initially amorphous Co(W,P) became gradually replaced with a mixture of IMC phases; the polycrystalline structure was hence observed.

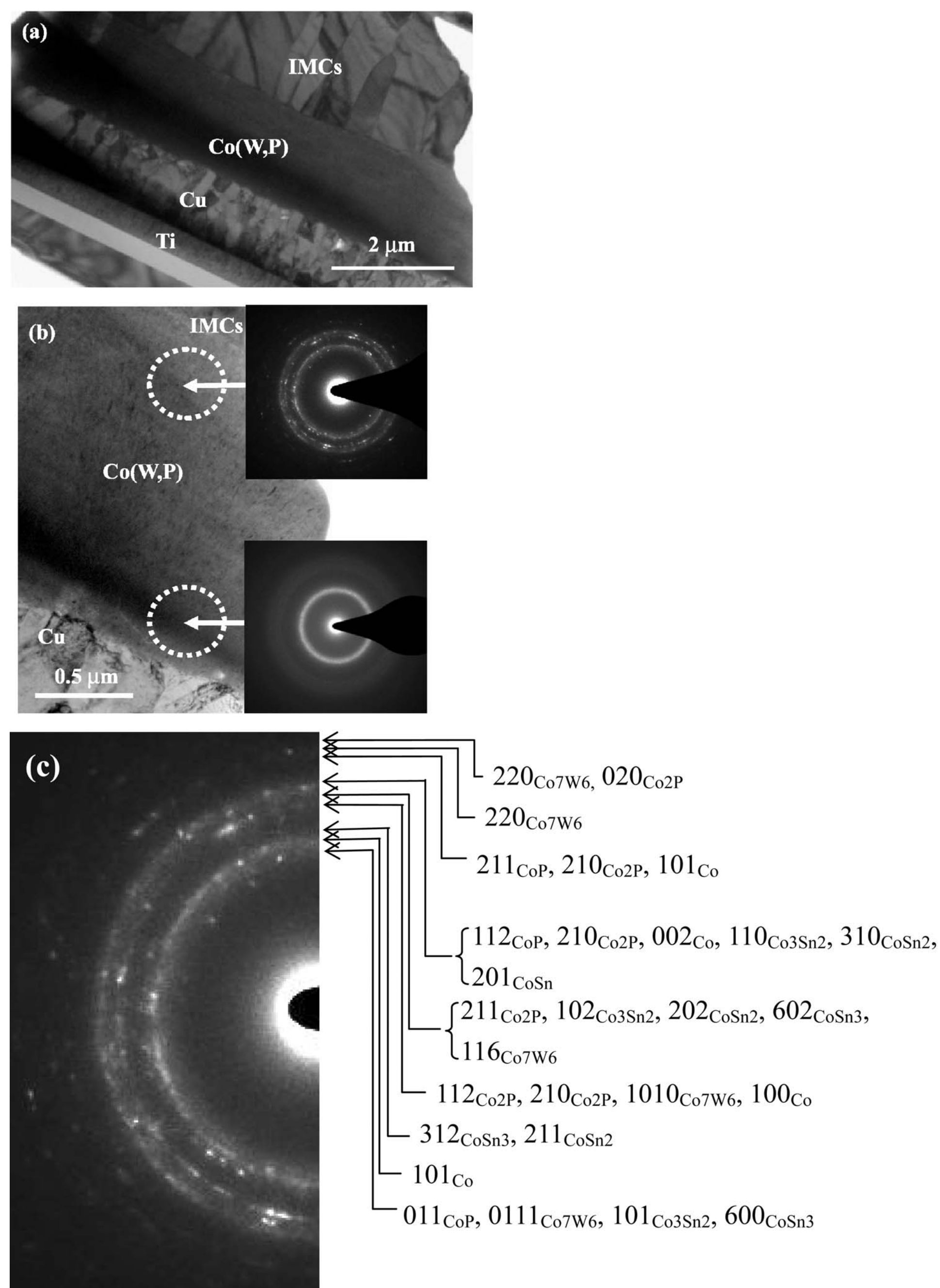

Figure 12. XTEM images of (a) the sample subjected to solid-state aging for 1000 h and (b) an enlarged portion of the Co(W,P) layer. The dotted circles in (b) specify the areas at which the SAED patterns were recorded. (c) Index of the SAED pattern attached at the upper right side of (b). The ring locations for all possible IMC types are specified in terms of the Joint Committee of Powder Diffraction Standard data.

As revealed by the TEM analyses shown in Fig. 10 and 12b, the P-rich layers present in samples subjected to liquid- and solid-state aging tests are both polycrystalline. For those initially amorphous barrier layers, in practice they would become polycrystalline because of the heat associated with device assembly process and operation. Hence, to sustain the barrier capability, a specific type of barrier mechanism that can retard short-circuit diffusion in the polycrystalline structure must be present. In the case of electroless Co(W,P), it becomes the stuffed-type barrier as revealed in the above analytical results. The pursuit of an amorphous state seems thus not a crucial issue for electroless Co(W,P) when serving as the diffusion barrier. A similar inference might apply also to electroless Ni(P) that is widely adopted as the barrier layer in UBM.[4-7,21] Finally, unlike a sample subjected to liquid-state aging, the portion of Co(W,P) adjacent to the Cu underlayer remains mostly amorphous after a solid-state aging test for 1000 h; it effectively retards Cu diffusion through the lack of grain boundaries as depicted by EDX analysis shown in Fig. 11c. These results are convincing that electroless Co(W,P) provides an excellent barrier layer in UBM for flip-chip Cu–IC.

Conclusions

We investigated the plating characteristics of electroless Co(W,P) layers and its applicability to a UBM structure as a diffusion barrier layer for flip-chip Cu–IC. For a plating solution with pH in a range of 7.6–9.0, the hydroxyl ion-related kinetics proposed by Paunovic et al. dominated the plating that, in turn, depressed the rate of deposition of Co(W,P) when the pH was increased. Although the rate of plating was low, the deposition of Co(W,P) at large pH benefited the densification and surface flatness of the Co(W,P) layer. It also increased the P content in Co(W,P) that, in turn, induced Co(W,P) to become amorphous and assured its barrier capa-

bility. The present work indicates that electroless Co(W,P) layers become noncrystalline when the pH exceeds ~8.6, or the P content of the film is >9 atom %.

SEM/TEM/EDX analyses of the solder/Co(W,P)/Cu/Ti/Si samples subjected to liquid- and solid-state aging tests revealed that the electroless Co(W,P) effectively inhibits the interdiffusion of Sn and Cu elements. The superior barrier capability of electroless Co(W,P) is attributed mainly to the formation of a P-rich layer at the expense of alloy reactions of solder and Co(W,P) to retard further interdiffusion, and the aggregation of elemental P and W and/or the formation of IMC, such as Co_2P at the interfaces of nanograins in electroless Co(W,P) to suppress short-circuit diffusion along grain boundaries. According to the SEM/TEM/EDX analyses, the electroless Co(W,P) serves as a barrier of combined type, i.e., a combination of sacrificial and stuffed barrier, for UBM applications. Furthermore, the $CoSn_2$ dominated the spalled IMC type in the solder of the specimens subjected to liquid-state aging, whereas in samples subjected to solid-state aging, reactions of solder and Co(W,P) imply the formation of $CoSn_2$ and $CoSn_3$ IMCs. TEM analysis revealed that a netlike Co_2P structure forms in Co(W,P) of the specimen subjected to liquid-state aging whereas a mixture of complicated IMC phases constitutes the P-rich layer presented in the samples subjected to aging tests. The incorporation of W enhanced the barrier property of electroless Co(W,P). A thickness at least 2 μm is required for an electroless Co(W,P) layer to serve as a diffusion barrier layer in UBM for flip-chip Cu–IC.

Acknowledgments

Department of Industrial Technology, Ministry of Economic Affairs of ROC under Technology Development Program for Academic contract no. 95-EC-17-A-05-S1-020, and National Science Council of ROC under contract no. NSC94-2216-E-009-026 supported this work. The TEM/EDX analysis and the focused ion-beam technique for preparation of XTEM specimens supported by Materials Analysis Technology, Inc., Chupei, Taiwan, and editing of the original manuscript by Muh-Wang Liang are also deeply acknowledged.

National Chiao-Tung University assisted in meeting the publication costs of this article.

References

1. M.-A. Nicolet, *Thin Solid Films*, **52**, 415 (1978).
2. C.-Y. Lee, T.-H. Huang, and S.-C. Lu, *J. Mater. Sci.*, **9**, 337 (1998).
3. R. H. Uang, K. C. Chen, S. W. Lu, H. T. Hu, and S. H. Huang, *IEEE Electron. Packag. Technol. Conf.*, Singapore, Dec. 5–7, p. 292, IEEE, Piscataway, NJ (2000).
4. M.-W. Liang, T.-E. Hsieh, C.-C. Chen, and Y.-T. Hung, *Jpn. J. Appl. Phys., Part 1*, **43**(12), 8258 (2004).
5. T. Oppert, E. Zakel, and T. Teutsch, *Proc. IEMT/IMC Symp.*, Japan, April 15–17, p. 106, IMPAS/IEEE, CPMT JAPAN (1998).
6. T. Teutsch, T. Oppert, E. Zakel, and E. Klusmann, *Electron. Comp. and Technol. Conf.*, Las Vegas, p. 107, IEEE, Piscataway, NJ (2000).
7. G. O. Mallory and J. B. Hajdu, *Electroless Plating Fundametals and Applications*, Chap. 1–7, AESF, Noyes Publications/William Andrew Publishing, Norwich, NY (1990).
8. E. J. O'Sullivan, A. G. Schrott, M. Paunovic, C. J. Sambucetti, J. R. Marino, P. J. Bailey, S. Kaja, and K. W. Semkow, *IBM J. Res. Dev.*, **42**, 607 (1998).
9. S. T. Chen and G. S. Chen, *J. Electrochem. Soc.*, **151**, 99 (2004).
10. M.-W. Liang, H.-T. Yen, and T.-E. Hsieh, *J. Electron. Mater.*, **35**, 1593 (2006).
11. A. Kohn, M. Eizenberg, Y. Shacham-Diamand, and Y. Sverdlov, *Mater. Sci. Eng., A*, **A302**, 18 (2001).
12. A. Kohn, M. Eizenberg, Y. Shacham-Diamand, B. Israel, and Y. Sverdlov, *Microelectron. Eng.*, **55**, 297 (2001).
13. A. Kohn, M. Eizenberg, and Y. Shacham-Diamand, *Appl. Surf. Sci.*, **212**, 367 (2003).
14. N. Petrov, Y. Sverdlov, and Y. Shacham-Diamand, *J. Electrochem. Soc.*, **149**, C187 (2002).
15. M. Paunovic, T. Nguyen, R. Mukherjee, C. Sambucetti, and L. Romankiw, *J. Electrochem. Soc.*, **142**, 1495 (1995).
16. M. Paunovic and M. Schlesinger, *Fundamentals of Electrochemical Deposition*, 2nd ed., Wiley, New York (1998).
17. T. B. Massalski, Editor, *Binary Alloy Phase Diagrams*, 2nd ed., ASM International, Materials Park, OH (1990).
18. M. Jiang, J. Sato, I. Ohnuma, R. Kainuma, and K. Ishida, *CALPHAD: Comput. Coupling Phase Diagrams Thermochem.*, **28**, 213 (2004).
19. K. C. Hung, Y. C. Chan, and C. W. Tang, *J. Mater. Sci.*, **11**, 587 (2000).
20. K. Hono and D. E. Laughlin, *J. Magn. Magn. Mater.*, **80**, L137 (1989).
21. J. H. Lau, Editor, *Flip Chip Technologies*, McGraw-Hill, New York (1996).